



# ZIF-8 Vibrational Spectra: Peak Assignments and Defect Signals

## M. Ahmad, J. Boscoboinik

To be published in "ACS Applied Materials & Interfaces"

May 2024

### Center for Functional Nanomaterials

# **Brookhaven National Laboratory**

## **U.S. Department of Energy**

USDOE Office of Science (SC), Basic Energy Sciences (BES). Scientific User Facilities (SUF)

Notice: This manuscript has been authored by employees of Brookhaven Science Associates, LLC under Contract No.DE-SC0012704 with the U.S. Department of Energy. The publisher by accepting the manuscript for publication acknowledges that the United States Government retains a non-exclusive, paid-up, irrevocable, world-wide license to publish or reproduce the published form of this manuscript, or allow others to do so, for United States Government purposes.

### **DISCLAIMER**

This report was prepared as an account of work sponsored by an agency of the United States Government. Neither the United States Government nor any agency thereof, nor any of their employees, nor any of their contractors, subcontractors, or their employees, makes any warranty, express or implied, or assumes any legal liability or responsibility for the accuracy, completeness, or any third party's use or the results of such use of any information, apparatus, product, or process disclosed, or represents that its use would not infringe privately owned rights. Reference herein to any specific commercial product, process, or service by trade name, trademark, manufacturer, or otherwise, does not necessarily constitute or imply its endorsement, recommendation, or favoring by the United States Government or any agency thereof or its contractors or subcontractors. The views and opinions of authors expressed herein do not necessarily state or reflect those of the United States Government or any agency thereof.

## ZIF-8 vibrational spectra: Peak assignments and defect signals

Mueed Ahmad,<sup>a,b,‡</sup> Roshan Patel,<sup>c,d,‡</sup> Dennis T. Lee,<sup>a,e</sup> Peter Corkery,<sup>e</sup> Andrea Kraetz,<sup>e</sup> Prerna,<sup>c,d</sup> Samuel A. Tenney,<sup>b</sup> Dmytro Nykypanchuk,<sup>b</sup> Xiao Tong,<sup>b</sup> J. Ilja Siepmann,<sup>c,d,\*</sup> Michael Tsapatsis,<sup>e,f,\*</sup> and J. Anibal Boscoboinik<sup>a,b,\*</sup>

<sup>a</sup>Department of Materials Science and Chemical Engineering, Stony Brook University, Stony Brook, NY, USA

<sup>b</sup>Center for Functional Nanomaterials, Brookhaven National Laboratory, Upton, NY, USA

<sup>c</sup>Department of Chemistry and Chemical Theory Center, University of Minnesota, 207 Pleasant Street SE, Minneapolis, Minnesota 55455-0431, United States

<sup>d</sup>Department of Chemical Engineering and Materials Science, University of Minnesota, 421 Washington Avenue SE, Minneapolis, Minnesota 55455-0132, United States

<sup>e</sup>Department of Chemical and Biomolecular Engineering & Institute for NanoBioTechnology, Johns Hopkins University, Baltimore, MD, USA

fApplied Physics Laboratory, Johns Hopkins University, Laurel, MD, USA

KEYWORDS: ZIFs, MOFs, Vibrational Spectroscopy, Defects in ZIFs, Peak Assignments, IR Spectra

ABSTRACT: Zeolitic Imidazolate Framework-8 (ZIF-8) is a promising material for gas separation applications. It also serves as a prototype for numerous ZIFs, including amorphous ones, with a broader range of possible applications, including sensors, catalysis, and lithography. It consists of zinc coordinated with 2-methylimidazolate (2mIm) and has been synthesized with methods ranging from liquid-phase to solvent-free synthesis, which aim to control its crystal size and shape, film thickness and microstructure, and incorporation into nanocomposites. Depending on the synthesis method and post-synthesis treatments, ZIF-8 materials may deviate from the nominal defect-free ZIF-8 crystal structure due to defects like missing 2mIm, missing zinc, and physically adsorbed 2mIm trapped in the ZIF-8 pores, which may alter its performance and stability. Infrared (IR) spectroscopy has been used to assess the presence of defects in ZIF-8 and related materials. However, conflicting interpretations by various authors persist in the literature. Here, we systematically investigate ZIF-8 vibrational spectra by combining experimental IR spectroscopy and first-principles molecular dynamics simulations, focusing on assigning peaks and elucidating the spectroscopic signals of putative defects present in ZIF-8 material. We attempt to resolve conflicting assignments from the literature and to provide a comprehensive understanding of the vibrational spectra of ZIF-8 and its defect-induced variations, aiming towards more precise quality control and design of ZIF-8-based materials for emerging applications.

#### 1. INTRODUCTION

Metal-organic frameworks (MOFs) are porous materials composed of metal ions or metal-containing clusters linked by organic ligands that form three-dimensional networks with highly ordered pore structures. <sup>1-6</sup> Zeolitic imidazolate frameworks (ZIFs) are a subclass of MOFs, and ZIF-8 is a prototypical ZIF consisting of zinc cations tetrahedrally coordinated with 2-methylimidazole (2mIm) ligands to form an ordered structure with nm-sized porous cavities accessible through smaller pore windows. <sup>7</sup> It has been investigated in the form of powders, <sup>8, 9</sup> films, <sup>10-14</sup> and in composites <sup>15</sup> made by solvothermal and vapor-phase approaches, <sup>16-20</sup> for applications ranging from gas<sup>21</sup> and hydrocarbon mixture purification, <sup>22,23</sup> and storage, <sup>24,25</sup> catalysis, <sup>26</sup> drug delivery, <sup>27</sup> and sensors. <sup>28</sup>

Depending on the synthesis conditions and post-synthesis treatments, various types of defects can be introduced in ZIF-8, and its structure may deviate from the defect-free nominal crystallographic structure. Zhang et al.<sup>29</sup> reported a computational description of defects in ZIF-8 and proposed three possible cases: missing 2mIm, missing zinc, and dangling linker groups caused by Zn coordinating to other species like water molecules instead of 2mIm. They

computed activation energies for forming these defects, and they proposed that defects could form when ZIF-8 was exposed to water molecules at ambient condition. The introduction of water-terminated defect sites was reported by Cheng et al.<sup>30</sup> These defects can likely alter the performance of ZIFs. For example, Lee et al.31 reported that the performance of propane/propylene separation can be influenced by the ZIF-8 membrane synthesis method, likely due to differences in defects associated with such methods. They correlated the relatively poor long-term membrane stability of rapidly grown membranes to their more defective structure. In an another example, it was shown that vapor-phase synthesis based on the conversion of ZnO into ZIF-8 by exposing ZnO to 2mIm vapors can leave ZnO residues underneath the ZIF-8 layer.<sup>32</sup> Tian et al.<sup>33</sup> utilized X-ray photoelectron spectroscopy (XPS) to detect functional groups, such as carbonates, water/hydroxides, and unreacted zinc-oxide in ZIF-8. However, XPS is probing depths on the order of only a few nanometers and has limitations in identifying chemical structures.

Infrared (IR) spectroscopy provides complementary information, as the vibrational spectra contain peaks assignable to specific functional groups and atomic connectivity, while IR light probes much deeper into the material than the escape depth of the low energy electrons that dictate the

depth sensitivity of XPS. In addition to vibrational modes that that can be identified as typical to specific moieties (e.g.: C-H stretching in the methyl group, or in the ring), structures with long range order, such as ZIF-8, have characteristic phonon modes related to the collective vibration of the structure. In this way, IR spectra are rich in structural and chemical information providing a fingerprint of the material. Changes in this fingerprint can be correlated to structural or chemical changes as the material is subject to different treatments.<sup>34</sup> However, the interpretation of such changes is not straightforward and leads to conflicting assignments and discrepancies in the literature.<sup>35</sup> The combination of experimental and theoretical methods can provide a clearer picture of the correlation between IR spectra and structure, and potentially resolve such discrepancies.

In this study, we combine experimental infrared spectroscopy with first-principles computational methods to interpret the vibrational spectra of pristine ZIF-8, and structural variations resulting from the introduction of defects. We attempt to resolve conflicting assignments found in earlier literature and improve the understanding of the vibrational spectra associated with ZIF-8. The information presented here is anticipated to contribute to a better understanding of ZIF-8 structures and the effects their variation could have in emerging applications in diverse fields, including gas separation, catalysis, sensors, and lithography.

#### 2. MATERIALS AND METHODS

#### 2.1 Materials

2-methylimidazole (2mIm, 99%) was purchased from Sigma Aldrich. Diethylzinc (DEZ, 95%) was purchased from STREM chemicals. SSP Silicon wafers <100> and DSP Silicon wafers <111> were purchased from University Wafer Inc and used for synthesizing ZIF-8 films. Zinc acetate dihydrate (Zn(OAc) $_2$ ·2H $_2$ O) was purchased from Fisher chemical. Homemade Milli-Q DI-water was used. 200 proof Ethanol was purchased from VWR International. All chemicals were used without any further purification.

#### 2.2 Synthesis of ZIF-8 films

ZIF-8 films supported on Au-coated silicon wafers were synthesized using the vapor-based synthesis method introduced by Ameloot and co-workers  $^{16}$  and as described in our earlier work.  $^{36,37}$  The silicon wafers were coated with ca. 100 nm Au using a Lesker 75 PVD system. The Au-coated silicon wafers were then cut into 1 cm × 1 cm square pieces and were utilized as a support for ZIF-8 films. ZnO thin film deposition was performed on the square-sized pieces loaded into an atomic layer deposition (ALD) reactor (Savannah S200, Veeco Instruments Inc.). The deposition was performed by alternating between  $H_2O$  and Diethyl Zinc (DEZ) precursor pulses, each followed by an Ar purge. The sequence time for each " $H_2O$  pulse/Ar purge/DEZ pulse/Ar purge" cycle was set to 0.015/5/0.015/5 seconds, respectively. A total of 100 ALD cycles lead to a ca.13-15 nm ZnO

film, as confirmed by ellipsometry, using a Film Sense FS-1 Multi-Wavelength Ellipsometer.

Crystalline ZIF-8 films (hereafter ZIF-8 Film) were synthesized in a Teflon bottle. Initially, 0.2 g of 2mIm solid was placed at the bottom of a 60 mL Savillex Teflon bottle, and a drop of DI water (40 µL) was carefully added without touching the 2mIm solid. Subsequently, ZnO-coated substrates (prepared as described above) were placed on a Teflon pedestal inside the bottle. After closing the lid, the Teflon bottle was placed in a pre-heated oven at 120 °C and held for 20 hours. The Teflon bottle was then removed from the oven and allowed to cool in ambient condition. After cooling, the wafers were removed from the Teflon bottle and immersed in methanol for 15 minutes aiming to the removal of excess 2mIm remaining on the film surface. The ca. 150 nm thick films were then air-dried overnight under ambient conditions. The dried samples remained stored under ambient conditions until they were subsequently used for further analysis in IR studies.

Some crystalline ZIF-8 films were synthesized in a quartz reactor as described earlier<sup>38</sup> (hereafter ZIF-8<sub>q</sub> Film, with subscript q indicating quartz reactor). ZnO-coated substrates were placed on a stainless-steel mesh used as a sample holder inside a custom-built quartz reactor with 0.2 g of 2mIm solids (no water was added in these experiments). The quartz reactor was then flushed with Ar gas and evacuated for 15 min under dynamic vacuum. After that, the valve connecting the reactor to the vacuum pump was closed, followed by heating the reactor at 120 °C for four hours under static vacuum (~10 mbar). After the reaction, the reactor was cooled to room temperature. The produced ZIF-8 films (~150 nm thick) were rinsed by immersing them in methanol for 15 min and then air-dried overnight and stored under ambient conditions before taking any IR measurements.

#### 2.3 Synthesis of ZIF-8 powder

ZIF-8 powder was synthesized at room temperature following the method reported by Miyake et al.  $^9$  The molar ratio for Zn:2mIm:  $H_2O$  for the synthesis mixture used in this work was 1:100:2228. The average crystal size of obtained ZIF-8 powder was about  $\sim\!3~\mu m$ .

#### 2.4 Characterization Methods

Infrared reflection absorption spectroscopy (IRRAS) was performed on ZIF-8 films in ultra-high vacuum (UHV) conditions with a base pressure of <1 x  $10^{-8}$  mbar. The ZIF-8 films supported on Au-coated wafers were placed on a flagstyle steel sample plate. A thermocouple (type K) was spot welded next to the wafer for measuring sample temperature during heating. The IR spectra were collected using a Bruker Vertex 80V spectrometer equipped with a mercury-cadmium-telluride (MCT) detector, set at a grazing incidence angle of 8°. Spectra were collected over a 4000-800 cm<sup>-1</sup> range, with a resolution of 4 cm<sup>-1</sup>. The data were collected using the standard Bruker OPUS software package v8.1.

The Attenuated Total Reflectance Fourier Transform Infrared (ATR-FTIR) analysis was conducted for ZIF-8 powder using a ThermoNicolet Nexus 670 FTIR Spectrometer. The spectrometer was equipped with a KRS-5 ATR accessory featuring diamond and sapphire anvil fittings, along with a cover suitable for volatile samples.

The X-ray Diffraction (XRD) pattern for ZIF-8 powder was obtained using a Rigaku MiniFlex X-ray diffractometer. The measurements were conducted at 40 kV and 15 mA, utilizing a Cu K $\alpha$  source ( $\lambda$ =1.54 Å). The scan covered a 2-theta range from 5 to 50° with a step size of 0.02° and a scan rate of 1° per minute.

Grazing incidence X-ray diffraction (GIXD) measurements were performed for ZIF-8 films using a Rigaku Smartlab II setup. The X-ray source was operated at 40 kV and 45 mA using Cu K $\alpha$  radiation ( $\lambda$  = 1.54 Å) at a constant incidence angle of 0.18 degrees. The diffraction pattern was measured over a range of 5-40 degrees and at speed of 0.5 degree/minute with 0.04 degrees step size.

The X-ray photoelectron spectroscopy (XPS) spectra were obtained in ultrahigh vacuum (UHV) conditions, with a base pressure of  $\sim\!10^{\circ}\text{--}9$  mbar at room temperature. A SPECS electron spectrometer, featuring a PHOIBOS 100 hemispherical energy analyzer and a monochromatic Al K $\alpha$ x-ray source (1486.7eV), was utilized for data collection. Data analysis and fitting were performed using CasaXPS software.

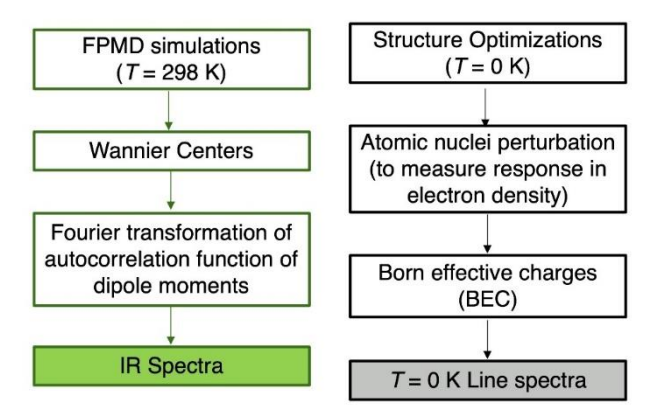
Atomic Force Microscopy (AFM) and AFM-IR data were collected on a Bruker Nano-IR3-s equipped with a quantum cascade laser at Brookhaven National Laboratory. Scans were collected in Tapping AFM-IR mode using Anasys Instruments PR-EX-TnIR-C-10 probes with a resonance frequency of 300kHz and a spring constant of 40N/m.

Scanning Electron Microscopy (SEM) images were captured by JEOL 1400F and Tescan Mira 3 GM SEM instruments, operating at voltages ranging from 2 to 10 kV.

# 2.5 Computation of Vibrational Spectra and Vector Plots

First principles molecular dynamics (FPMD) simulations were carried out for a single unit cell of ZIF-8 embedded in periodic boundaries. Given the computational demands of FPMD simulations and their unfavorable scaling with the system size, it is preferable to investigate a multitude of small systems containing a specific modification of the ZIF-8 structure and/or including adsorbed species instead of a larger system with multiple unit cells containing multiple types of defects. Here, we considered the following four systems: (a) defect-free ZIF-8, (b) missing-Zn defect in ZIF-8, containing a missing Zn node replaced by two protons, (c) missing-2mIm defect in ZIF-8 containing a missing imidazolate linker replaced by H2O and OH- species, and (d) additional-2mIm in ZIF-8, containing two 2mIm molecules in the pore of defect-free ZIF-8. The CP2K software package<sup>39</sup> was used for the FPMD simulations in the canonical (NVT) ensemble (T = 298 K). We employed the Perdew-Burke-Ernzerhof (PBE) functional<sup>40</sup> along with D3 dispersion corrections by Grimme<sup>41</sup>. The basis set used for Zn, C, H, O, and N, was DZVP-MOLOPT-SR-GTH,42 with PBE pseudopotentials

of the Goedecker-Teter-Hutter (GTH) analytical form<sup>43</sup>. A planewave cutoff energy of 600 Ry was used, and the target accuracy of 10<sup>-6</sup> Ha was used for the self-consistent field (SCF) calculations. The length of the simulations was 5 ps for each structure with a time step of 0.5 fs. The last 3 ps were used for computation of the vibrational spectra. To obtain the vibrational spectra, we used the approach of Wannier localization<sup>44</sup>, wherein we calculated the centers of maximally localized Wannier functions every 2.5 fs on-thefly and constructed the system dipoles using the Wannier centers. The "Crazy Angle algorithm" implemented in CP2K (rather than Jacobi diagonalization) was utilized to construct a suitable unitary transformation of the molecular orbitals. The  $TRAVIS^{45}$  tool was used to evaluate the Fourier transform of the autocorrelation functions of the system dipole moments and obtain the vibrational spectra at 298 K. In addition to the FPMD simulations, we also carried out density functional theory-based geometry optimization (T =0 K) of single unit cells using the Vienna Ab initio Simulation Package (VASP)46,47 and the PBE functional. Frequency calculations were performed to obtain the vibrational modes, and corresponding vibrational IR spectra intensities were computed using Density-Functional Perturbation Theory (DFPT). This approach yields the line spectra at T = 0 K. The displacement vectors for the vibrational modes corresponding to different peaks allow for the visualization of the vibrational modes. The two complementary approaches are summarized in Scheme 1. The unit cell sizes for different simulation cases were kept the same (16.991 Å), as reported by Park et al.7



Scheme 1: Computational workflow for obtaining the vibrational spectra from FPMD (at T = 298 K) and the line-plot based on DFT (at T = 0 K).

#### 3. RESULTS AND DISCUSSION

Figure 1 displays IR spectra in the range of 1700-900 cm<sup>-1</sup> obtained by several authors for different forms of ZIF-8. Additional information about these previously reported IR spectra can be found in Table S1. It is evident that there are differences among these IR spectra. Moreover, the assignment of the peaks to vibrational modes differs among these studies.

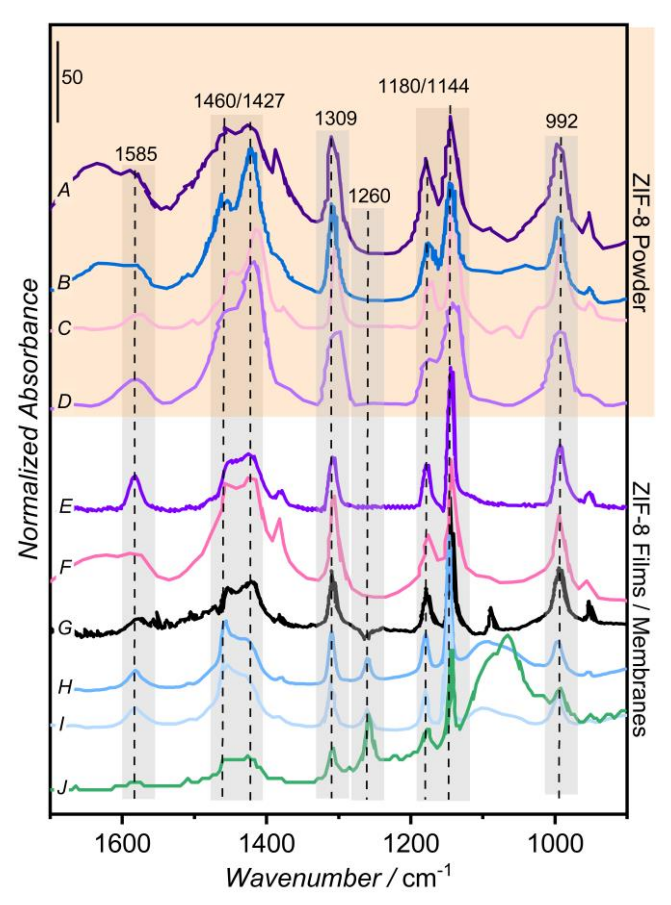


Figure 1: Previously reported IR spectra for ZIF-8 Powder (Spectra A - Zhang et al.,<sup>48</sup> B - Liu et al.,<sup>49</sup> C - Nozari et al.,<sup>50</sup> and D - Silva et al.,<sup>51</sup> ) and ZIF-8 Films/Membranes (Spectra E - Zhao et al.,<sup>52</sup> F - Nordin et al.,<sup>53</sup> G - Tian et al.,<sup>33</sup> H - Miao et al.,<sup>38</sup> I - Mello et al.,<sup>37</sup> and I- Kräuter et al.<sup>54</sup>).

Zhang et al. 48 (spectrum A) assigned the peaks at 1145 cm<sup>-</sup> <sup>1</sup>, 1300-1460 cm<sup>-1</sup>, and 1585 cm<sup>-1</sup> to the C-N stretching, entire imidazole ring stretching, and C=N stretching modes, respectively. They also reported a peak at 1635 cm<sup>-1</sup> and assigned it to C=C stretching modes. However, Liu et al.49 (spectrum B) assigned only the peaks in the 1100-1400 cm <sup>1</sup> range to the C-N stretch mode, and did not report any peak around 1635 cm<sup>-1</sup>. Nozari et al.<sup>50</sup> (spectrum C) assigned a broad IR range to groups of vibrational modes such as the entire 1700-800 cm<sup>-1</sup> to in-plane bending and the entire imidazole ring stretching modes. Silva et al.51 (spectrum D) assigned the peaks at 1457, 1423 and 1145 cm<sup>-1</sup> to C-N and C=N vibrational modes. But, Zhao et al.  $^{52}$  (spectrum E) assigned the 1456 cm<sup>-1</sup> peak to in-plane vibration of -CH<sub>3</sub>. They also assigned the peaks around 1580 cm<sup>-1</sup> to C=N stretches in agreement with other authors. 48,49,51,52 However, Xu et al.55 disagree with this assignment based on their simulations as we will discuss below. Nordin et al. 53 (spectrum F) assigned the 1584 cm<sup>-1</sup> peak to C=N stretches and broadly assigned the 1350-1500 cm<sup>-1</sup> range to the entire imidazole ring stretching, which is not in agreement with the assignment reported by Zhao et al. 52 Tian et al. 33 (spectrum G) reported detailed peak assignments including 1574 cm<sup>-1</sup> to C=N stretch, 1473 cm<sup>-1</sup> & 1418 cm<sup>-1</sup> to -CH<sub>3</sub> bending modes, 1147 & 1180 cm<sup>-1</sup> to C-N in-plane stretching and

1311 & 954 cm<sup>-1</sup> to imidazole ring C-H bending modes. However, the assignment of the peak at 1091 cm<sup>-1</sup> to C-N symmetric stretch contradicts recent observations made by Kräuter et al.<sup>54</sup> as they attribute it to Si-O stretches coming from the native oxide of the silicon substrate. We also included ZIF-8 IR results reported earlier by our group (Miao et al. <sup>38</sup> and Mello et al. <sup>37</sup>) (spectra H & I) where peaks around 1400 cm<sup>-1</sup> were assigned to -CH<sub>3</sub> bending modes and the 1585 cm<sup>-1</sup> peak to C=N stretch. We also observed an additional peak around 1260 cm<sup>-1</sup> (as shown in spectra *H* & *I*) , similar to results reported by Stassen et al. 16 and Kräuter et al.<sup>54</sup> Results reported by Kräuter et al.<sup>54</sup> (spectrum /) have also a broad feature around 1090 cm<sup>-1</sup> in addition to the 1260 cm<sup>-1</sup> peak and were interpreted as Si-O peaks coming from the native oxide of the substrate, an assignment which will be discussed below in view of our findings.

Figure 2 presents simulated ZIF-8 IR spectra reported by different authors (see Table S2 for details). Xu et al.<sup>55</sup> (spectrum  $\alpha$ ) reported a comparison of simulated with experimentally obtained IR spectra from ZIF-8 powder and suggested that the peaks around 1300 cm<sup>-1</sup> and 1450 cm<sup>-1</sup> could originate from C=N stretching, which contradicts other authors who assigned 1585 cm<sup>-1</sup> to C=N stretching. <sup>48,49,51,52</sup> In their simulations, Xu et al.55 did not observe any peak at 1585 cm<sup>-1</sup>. Möslein et al.<sup>56</sup> reported simulated IR results for defect-free ZIF-8 (spectrum  $\beta$ ) as well as defective ZIF-8, along with experimental IR results. They did not observe any peak around 1585 cm<sup>-1</sup> from *defect-free* ZIF-8, which is in agreement with the results reported by Xu et al.55 while in the presence of missing-Zn defects, they reported additional peaks around 1115 cm<sup>-1</sup>, which they assigned to -C-N-H bending (made possible by the presence of H bound to N, when *missing-Zn* defects are present). In the presence of missing-2mIm defects, they reported additional peaks at 1250 cm<sup>-1</sup> and 1350 cm<sup>-1</sup>. Xiong et al.<sup>57</sup> (spectrum  $\gamma$ ) also reported a simulated IR spectrum of ZIF-8 and suggested that the 1310 cm<sup>-1</sup> peak be attributed to in-plane antisymmetric ring stretching, which is in contradiction with the results reported by Xu et al.<sup>55</sup> who assigned the 1307 cm<sup>-1</sup> peak to C=N stretching.

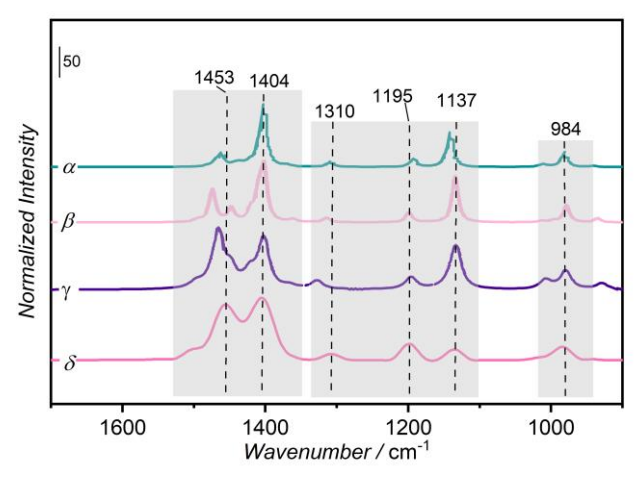


Figure 2: Simulated IR spectra for *defect-free* ZIF-8 reported by different authors (Spectrum  $\alpha$  – Xu et al.<sup>55</sup>,  $\beta$  - Möslein et al.<sup>56</sup> &  $\gamma$  - Xiong et al.<sup>57</sup>) and in this work (Spectrum  $\delta$ ).

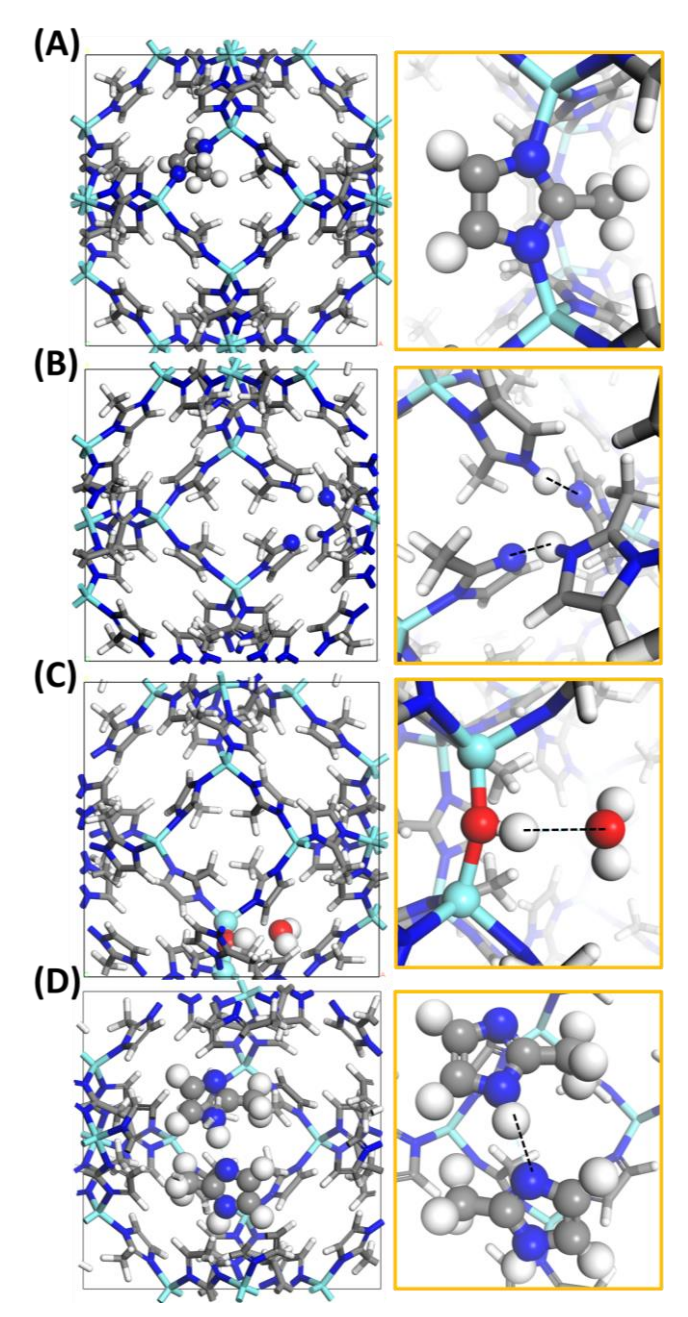


Figure 3: Simulated ZIF-8-unit cells: (A) *defect-free* ZIF-8, with (B) *missing-Zn* defect, (C) *missing-2mIm* defect, and (D) two *additional-2mIm* molecules inside ZIF-8 pores. (Color Scheme: Cyan - Zinc, Blue - Nitrogen, Grey - Carbon, Red - Oxygen, White - Hydrogen; The dotted lines in 2B (right), 2C (right) and 2D (right) represent hydrogen bonding)

In an attempt to settle these differences in vibrational mode assignments for ZIF-8, we modeled four ZIF-8 structures (shown in Figure 3): defect-free (3A), missing-Zn defect (3B), missing-2mIm (3C), and ZIF-8 with additional-2mIm in the pores (3D). Figure 3A presents a unit cell of defect-free ZIF-8 (left) and a close-up (right) of a deprotonated 2mIm molecule (2mIm anion) coordinated to two Zn atoms. Each unit cell has twelve Zn atoms, and one zinc atom was removed to model a missing-Zn defect. The missing-Zn defect is presented in Figure 3B; a unit cell view is given on the left while a close-up image is shown on the right highlighting, along

with the missing Zn<sup>2+</sup> cation, four nitrogen atoms from four 2mIm ligands, two of which are protonated to maintain charge neutrality. For the *missing-2mIm* defect (shown in Figure 3C), we removed one negatively-charged 2mIm linker which leads to two undercoordinated Zn sites. To achieve charge neutrality and to coordinate the two Zn sites, we added one hydroxide (OH-) anion and one water molecule, as suggested by Möslein et al.<sup>56</sup> However, during the MD simulations, the water attached to Zn atom detaches and an -OH bridge forms between the two Zn atoms as shown in Figure 3C. We also modeled ZIF-8 with two trapped 2mIm molecules inside its pore to simulate extra-framework additional-2mIm, as shown in Figure 3D.

Figure 4 presents simulated IR spectra at 298 K along with atomic displacement vector plots corresponding to each position for each variant of ZIF-8 shown in Figure 3. Figure S1 shows the corresponding line-plots at 0 K. The comparison of our simulated IR spectrum for defect-free ZIF-8 is also included as Spectrum  $\delta$  in Figure 2. The simulated peak positions largely match the reported results from previous literature. In addition to the simulated IR spectra, animation files for each vibrational mode corresponding to each variant of ZIF-8 are provided in the Supporting Information. We would like to emphasize that vibrational modes are more complex than what is typically described in words as a relative motion of two atoms (i.e., bond stretching) or of three atoms (i.e., angle bending) or by displacement vectors for individual atoms. Thus, we strongly encourage the reader to watch the animations associated with these regions or modes (see Supporting Information Files) to complement the text. Below, we offer a detailed peak-by-peak assignment to vibrational modes based on our simulation results.

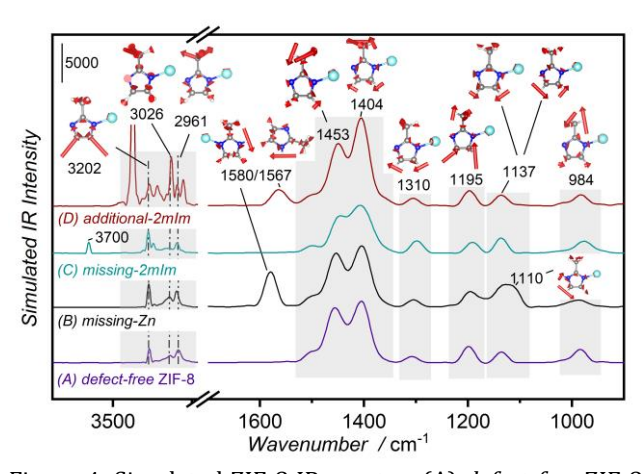


Figure 4: Simulated ZIF-8 IR spectra: (A) *defect-free* ZIF-8, (B) *missing-Zn* defect, (C) *missing-2mIm* defect, and (D) two *additional-2mIm* molecules inside ZIF-8 pores. Cartoons on top represent atomic displacement vector plots corresponding to each peak position (line-break is from 1700 to 2800 cm<sup>-1</sup>; full range without break is provided in Figure S2), Same color scheme for atoms as in Figure 3.

#### 3.1 Vibrational mode assignments

In the following paragraphs, we will discuss the different regions of the spectrum in order of ascending frequency, including experimental results, simulations, and their comparison with the literature and we will provide our

proposed assignments. We emphasize that vibrational modes are typically more complex than what words or a vector can describe. Therefore, we provide animations associated with these regions or modes to complement the text. These are included in the Supporting Information and were simulated based on the density functional theory calculations.

3.1.1 Vibrational modes associated with *defect-free* ZIF-8

Vibrational modes at 990 cm<sup>-1</sup>

We propose the feature at 990 cm $^{-1}$  (centered at 984 cm $^{-1}$  in the simulations and observed near 992 cm $^{-1}$  in experiments) is due to a combination of C-H<sub>m</sub> (H<sub>m</sub> represents an H atom from the methyl group) bending modes from C-CH $_3$  along with in-plane C-H<sub>r</sub> rocking in the H<sub>r</sub>-C-C-H<sub>r</sub> (H<sub>r</sub> represents an H atom from the imidazole ring) moieties. The animation corresponding to these vibrational modes is included in the Supporting Information (labeled as "985\_defect\_free"). This peak has been observed in previous reports without assignment to a specific vibration. The alient to a specific vibration. We also observe a small in-plane deformation of the ring, as can be seen in the animation file. Prior simulations by Xu et al. The animation is the simulations of the ring as can be seen in the animation file.

Vibrational modes around 1100-1200 cm<sup>-1</sup>

We suggest that the feature around 1140 cm $^{-1}$  (centered at 1144 and 1137 cm $^{-1}$  in the experiments and FPMD simulations, respectively and representing multiples lines near 1145 cm $^{-1}$  in the static calculations) arises from combined scissoring and rocking motions of C-H $_{\rm r}$  in the H $_{\rm r}$ -C-C-H $_{\rm r}$  moieties of different 2mIm within a unit cell of ZIF-8. Note that some linkers within the unit cell show the rocking while others show the scissoring mode. From the multiple lines in this region from the static calculations, we compared the four with the highest intensities in the zero-K line spectrum (1144.2, 1145.4, 1145.5, and 1146.2 cm $^{-1}$ ) and found that they all correspond to small variations of the same vibrational mode (as illustrated in the corresponding animation file labeled as "1145\_defect\_free" in the Supporting Information).

Another feature around 1200 cm $^{-1}$  (centered at 1180 and 1195 cm $^{-1}$  in the experiments and FPMD simulations, respectively) involves bending modes from C-H $_{\rm f}$  with respect to the ring as well as breathing of the entire ring (including C-N vibrations). Minor C-H $_{\rm m}$  bending modes from C-CH $_{\rm 3}$  were also observed in this region. Although these peaks have been assigned to C-N stretching modes in previous literature,  $^{33,48,58}$  it should be noted that these assigned vibrational modes are a simplification because, as can be seen in the animation file (labeled as "1210\_defect\_free" in Supporting Information), they include more complex combinations involving multiple vibrational modes.

Vibrational mode at 1310 cm<sup>-1</sup>

We propose that the peak at 1310 cm $^{-1}$  (at 1310 cm $^{-1}$  for simulations and at 1309 cm $^{-1}$  in experiments) can be assigned to rocking mode of C-H $_{\rm r}$  in the H $_{\rm r}$ -C-C-H $_{\rm r}$  moieties, which agrees with the assignment by Tian et al.<sup>33</sup> A small deformation in the ring was also observed in this region, as shown in animations file labeled "1320\_defect\_free" in the Supporting Information.

Vibrational modes around 1400-1500 cm<sup>-1</sup>

The broad feature in this region presents two major peaks, one at 1400 cm<sup>-1</sup> (present at 1404 cm<sup>-1</sup> in simulations and at 1427 cm<sup>-1</sup> in experiments) and another at 1450 cm<sup>-1</sup> (observed at 1453 cm<sup>-1</sup> in FPMD simulations and at 1460 cm<sup>-1</sup> in experiments). A shoulder at 1500 cm<sup>-1</sup> is also observed. The corresponding atomic displacement vectors are dominated by the vibrational modes associated with C-H<sub>m</sub> bending modes from C-CH<sub>3</sub> with minor contributions from H<sub>r</sub>-C-C-H<sub>r</sub> rocking modes. We also observe ring deformation, partly in agreement with reports by Zhang et al.48 and Liu et al.,49 who have assigned 1300-1460 cm-1 to entire ring stretching modes and 1100-1400 cm<sup>-1</sup> to C-N stretches. Our assignment also agrees with Zhao et al.,52 as they have assigned the peak at 1453 cm<sup>-1</sup> to -CH<sub>3</sub> vibrational modes. The animation file corresponding to vibrational modes in this region is included in Supporting Information and labeled as "1400\_defect-free".

We also note that the relative intensities of the bands in this region differ between various experimental measurements and varies for powder and film samples (see Figure 1) with the powder samples mostly yielding higher intensity for the band at  $1427~\rm cm^{-1}$ . Relative peak intensities in this region also differ between defect-free and defective structures. Beyond defects, another possible reason could be variations in the lattice parameter for thin films compared to the ideal structure. Exploratory geometry optimizations for a unit cell with a 2% smaller lattice parameter yield a reduction in the intensities at  $\sim\!1420~\rm cm^{-1}$  and increased intensities around  $1460~\rm cm^{-1}$  compared to those with the regular unit cell size.

Vibrational modes around 3000 cm<sup>-1</sup>

Consistent with earlier reports, <sup>48,49,59</sup> we assign C-H<sub>m</sub> methyl group's symmetric and asymmetric stretches to 2960 cm<sup>-1</sup> (present at 2961 cm<sup>-1</sup> in simulations and at 2929 cm<sup>-1</sup> in experiments, animation file labeled as "2972\_defect\_free" in supporting information) and 3020 cm<sup>-1</sup> (centered at 3026 cm<sup>-1</sup> in simulations and at 2963 cm<sup>-1</sup> in experiments, animation file labeled as "3023\_defect\_free" in Supporting Information), respectively.

Vibrational modes around 3200 cm<sup>-1</sup>

We assign the peak in this region (centered at 3202 cm<sup>-1</sup> in simulations and observed at 3133 cm<sup>-1</sup> in experiments) to stretching modes from C-H<sub>r</sub> ring (as presented in animation

file labeled as "3202\_defect\_free" in Supporting Information) which is in agreement with reports by Zhang et al.,<sup>48</sup> Liu et al.,<sup>49</sup> and others.<sup>55</sup>

3.1.2 Vibrational modes associated with defects in ZIF-8 and additional 2mIm in ZIF-8 pores

Here, we attempt to explain additional peaks present in ZIF-8 simulated IR spectra when missing Zn or 2mIm defects or additional 2mIm are introduced.

Vibrational modes associated with ZIF-8 with *missing-Zn* defect (1100, 1580, 2000-2600 cm<sup>-1</sup>)

Because one missing Zn atom results in four dangling 2mIm (two of which present an N and two an NH), N-H···N bonding may occur between the N-H and the N from two 2mIm, as indicated by the dotted line in Figure 3B. This results in additional peaks that we report here and can be utilized as a signature for identifying missing-Zn defects in ZIF-8 as well as other ZIFs. A comparison of simulated IR plots corresponding to defect-free ZIF-8, and ZIF-8 with missing-Zn defect shows broad features at 1110 cm<sup>-1</sup> and an additional peak at 1580 cm<sup>-1</sup>. We propose that the broad feature we observe at 1110 cm<sup>-1</sup> can be assigned to -C-N-H bending modes,60 as shown in the animation file labeled as "1110\_missing\_Zn" in the Supporting Information. This observation agrees with results reported by Möslein et al.<sup>56</sup> We also propose that this peak includes contributions from bending modes of C-H<sub>r</sub> in the H<sub>r</sub>-C-C-H<sub>r</sub> moieties, similar to the vibrational modes at 1137 cm<sup>-1</sup> in *defect-free* ZIF-8. The peak at 1580 cm<sup>-1</sup> can be attributed to -NH bending from -CNH moiety of a dangling linker, as shown in Figure 4 and as illustrated in animation file labeled as "1586\_missing\_Zn" in the Supporting Information. We also observed an additional set of peaks around 2600-2000 cm<sup>-1</sup>, which were not present in *defect-free ZIF-8*, as shown Figure S2. The corresponding atomic displacement vector plots are presented in Figure S3. The peaks at the 2500 cm<sup>-1</sup> region can be assigned to -NH stretching vibrations, as illustrated in the animation file labeled as "2506\_missing\_Zn" and "2588\_missing\_Zn" in the Supporting Information. This frequency is significantly lower than expected for a N-H stretching mode (~3400 cm<sup>-</sup> 1), likely due to the elongation of the N-H bond due to N-H..N hydrogen bonding.61,62 Figure S4 shows that the N-H bond length increases from 1.015 Å in isolated 2mIm molecule, to ~1.048 Å (H atom in N-H..N) for the additional 2mIm defect case, and to ~1.080 Å for the missing-Zn defect case (H atom in N-H..N). In the missing-Zn defect case, we also observed that the hydrogen atom can hop from one N atom to another during our FPMD simulations as shown in the movie file labeled as "Movie File-1" in the Supporting Information.

Vibrational modes associated with ZIF-8 with *missing-2mIm* defect (3700 cm<sup>-1</sup>)

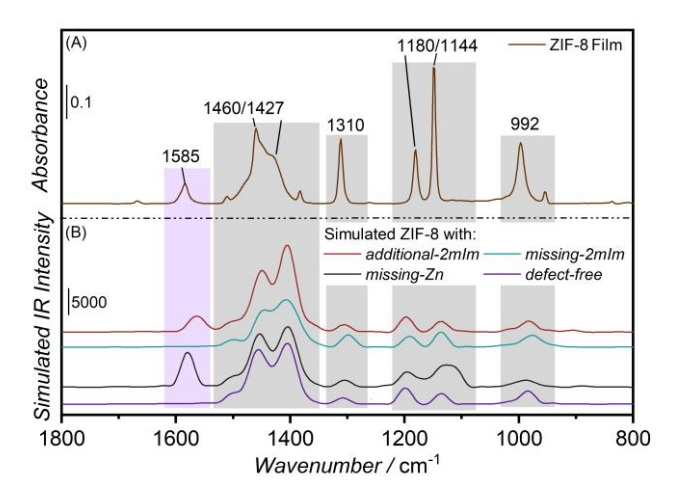
In the *missing-2mIm* defect case, we replace one 2mIm linker with one -OH group and one water molecule bound to two Zn atoms (one to each), similar to that reported by

Möslein et al. <sup>56</sup> During our FPMD simulations (T = 298 K), we noticed significant motion of the water molecule, indicating that it is loosely bound. The H<sub>2</sub>O bound to one of the two Zn atoms detaches from it, and the -OH bound to the other Zn atom bridges the two Zn atoms and results in -OH bridging within the first 2.5 ps of the trajectory as shown in the movie file labeled as "Movie File-2" in the Supporting Information. For this reason, the IR spectrum obtained from FPMD simulations, shown in Figure 4, is for the case where the loosely bound H<sub>2</sub>O molecule is not present. Using DFT geometry optimizations (T = 0 K), we obtained two structures, one where a water molecule and an -OH group are bound to two Zn atoms (and form a HOH-OH bridge between the two Zn atoms) and another, where the water molecule is detached from the Zn atom and an -OH bridges two Zn atoms, with the former being 51 kJ/mol (4.3 kJ/mol per Zn) lower in energy. Figure S5 compares the line plots for both static structure configurations corresponding to missing-2mIm defects and does not show additional peaks between 1250-1350 cm<sup>-1</sup> for either case, as reported by Möslein et al.<sup>56</sup> As stated before, we observed -OH bridging between two Zn atoms from the missing-2mIm simulated structure and we report an additional peak at 3700 cm<sup>-1</sup> that can be assigned to -OH stretches (as shown in Figure S3 and in animation file labeled as "3700\_missing\_2mIm").

Vibrational modes associated with ZIF-8 with *additional-2mIm* in its pores (1567, 2900-3400 cm<sup>-1</sup>)

We simulated the additional-2mIm case, to investigate trapped unreacted 2mIm in ZIF-8 by introducing two 2mIm molecules inside the pore of defect-free ZIF-8. These extra molecules may arise in practice due to trapped 2mIm during the synthesis process. The two 2mIm molecules interact with each other via a hydrogen bond (N-H...N). A peak at 1567 cm<sup>-1</sup>, which is not present in defect-free ZIF-8, can be assigned to -C-N-H bending modes with the H atom participating in hydrogen bond between two additional 2mIm molecules (as shown in the animation file labeled as "1575\_additional\_2mIm" in the Supporting Information). This peak is absent for the case when only a single 2mIm molecule, devoid of N-H...N hydrogen bonding, is present inside a ZIF-8 pore (see 1-additional-2mIm spectra in Figure S2). For the additional-2mIm case, we also observed additional peaks in the 2900-3400 cm<sup>-1</sup> region, apart from the already existing peaks at 3202 and 3026 cm<sup>-1</sup> seen in *defect*free case. For these additional 2mIm molecules, N-H stretching modes are observed at 3339 cm<sup>-1</sup> (for the -NH not involved in hydrogen bonding) and 2922 cm<sup>-1</sup> (for the -NH involved in hydrogen bonding). The animation files corresponding to the 3339 and 2922 cm<sup>-1</sup> -NH stretching modes are included in the Supporting Information and are labeled as "3400\_additional\_2mIm" and "2981\_additional\_2mIm", respectively. The lower frequency of 2922 cm<sup>-1</sup> (vs. 3339 cm<sup>-1</sup>) for the NH stretch involved in hydrogen bonding is in line with slightly longer N-H bond length of  $\sim 1.05$  Å (vs 1.02 Å; see Figure S4(B) for bond lengths). Also note that for the case of a single 2mIm inside a ZIF-8 pore, the frequency at 2922 cm<sup>-1</sup> is not observed, because of the absence of NH...N hydrogen bonding interaction. Apart from the 3202 cm<sup>-1</sup> peak assigned to the stretching modes of C-H<sub>r</sub> (seen also in

the defect free case), an extra peak at 3134 cm<sup>-1</sup> is present for the additional-2mIm case, corresponding to the stretching modes from C-H<sub>r</sub> but with the ring H<sub>r</sub> atom of the linker interacting with the N atom of the 2mIm molecule (as presented in the animation file labeled as "3140\_additional 2mIm" in the Supporting Information; the distance between the H atom of CH<sub>r</sub> and the N from 2mIm is 2.34 Å from the geometry-optimized structure). The simulated IR intensity can be correlated with the number of functional groups present in the simulated system. For example, we see an increased intensity around 1450 cm<sup>-1</sup> for the additional-2mIm case as opposed to reduced intensity when one linker was removed from the unit cell, as in the case of missing-2mIm defect. This behavior can be attributed to the number of methyl groups (-CH3) present in the simulated unit cell structure.



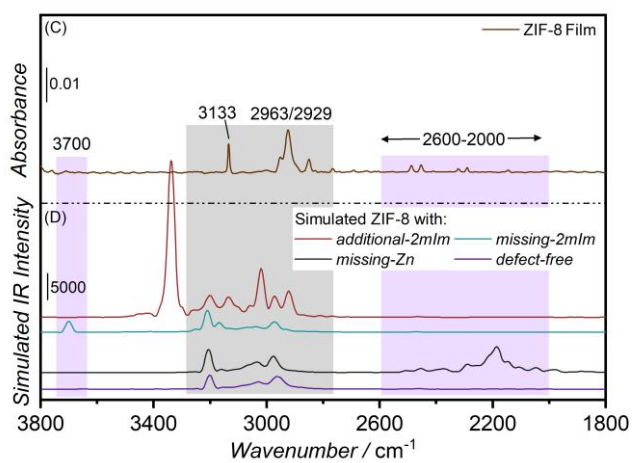


Figure 5: (A and C) Experimental IRRA spectrum of ZIF-8 films (made by vapor phase conversion of ZnO-coated substrates), and (B and D) simulated ZIF-8 IR spectra for *defect-free* ZIF-8 & ZIF-8 with *missing-Zn* defect, *missing-2mIm defect*, and two *additional-2mIm* in ZIF-8 for the 1800-800 cm<sup>-1</sup> (A and B) and the 3800-1800 cm<sup>-1</sup> (C and D) ranges.

#### 3.2 On the IR spectra of vapor phase deposited ZIF-8 Films

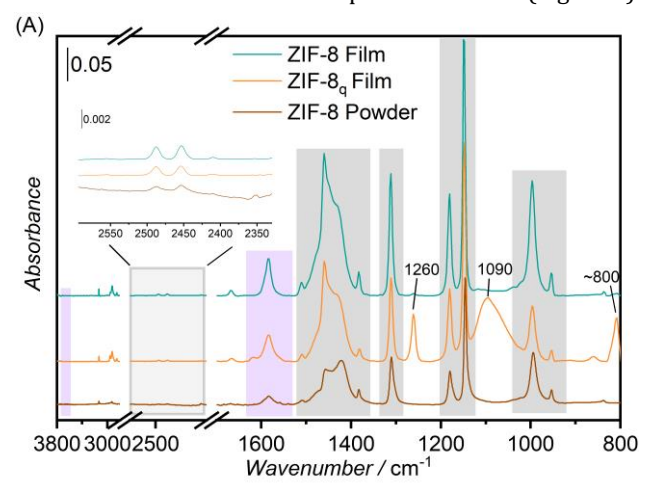
In Figure 5, the simulated IR plots, for the 3800-800 cm<sup>-1</sup> wavenumber range, are compared with the experimental IR

spectrum obtained from a ZIF-8 film (synthesized by treating ZnO-coated substrates with 2mIm and water vapors in a Teflon bottle). While we observe that the experimental IR results closely match the simulated results for a defect free structure, we observed an additional peak at 1585 cm<sup>-1</sup> (Figure 5 (A)), which was also reported previously by other authors. 48,49 Interestingly, IRRA spectra of ZIF-8q (q, for quartz reactor-see Materials and Methods section) film as well as ZIF-8 powder also exhibit the peak at 1585 cm<sup>-1</sup> as presented in Figure 6(A). Further investigation revealed the presence of additional set of peaks around 2500 cm<sup>-1</sup>, shown in Figure 6 (A, inset). The peaks around 2500 cm<sup>-1</sup> along with the peak at 1585 cm<sup>-1</sup> agree with our simulation results from the missing-Zn defect case and suggest the presence of missing-Zn defects in the ZIF-8 films and powder used in our study. The 1585 cm-1 peak has been reported in experiments by several authors<sup>48,49</sup> but it has not been observed in our simulations of defect-free ZIF-8, nor by defect-free simulations of other authors.55,56 As discussed above, we assigned this peak to -CNH in-plane bending modes from -NH created due to the missing-Zn. As explained earlier, the vibrations at 2600-2000 cm<sup>-1</sup> can be assigned to -NH stretches in *missing-Zn* defect case where one hydrogen is shared by two nitrogen atoms resulting in a weaker bond. Further, we do not observe any peak around 3700 cm<sup>-1</sup> from experimental IRRA spectra for ZIF-8 film (Figure 5 (C), Figure 6(A)) and thus cannot detect the presence of missing-2mIm defect sites in the ZIF-8 films or ZIF-8 powder. Further, a minor peak around 1650 cm<sup>-1</sup> is also observed from experimental as well as simulation results. Our calculations suggest that this peak corresponds to in-plane bending of -CH<sub>ring</sub>. An animation file for this peak, labeled as "1650\_defect free", is included in the Supporting Information. We also observed minor peaks at around 1500 cm<sup>-1</sup> and 1400 cm-1 in the experimental spectra. We propose that these peaks correspond to bending of methyl group along with bending modes from -CH<sub>ring</sub>. The animation file for set of vibrational modes around this region are provided as "1400-1500\_defect\_free" in the Supporting Information.

Further, Zn-N stretches have been previously reported around 420 cm<sup>-1</sup>.63,64 However, our simulations agrees with report by Xu et al.55 who have assigned the peak around 420 cm<sup>-1</sup> to bending mode of methyl group and imidazole ring. It is acknowledged that bending or stretching of the imidazole ring may cause changes in the relative positioning of N with respect to Zn. The animation file corresponding to vibration mode around 420 cm<sup>-1</sup> are included as "420\_defect\_free" in Supporting Information. Due to limitations from optical components in our experimental setup, we could not obtain IR spectra below 800 cm<sup>-1</sup> experimentally. SEM images and XRD patterns of ZIF-8 films and powder used herein are characteristic of ZIF-8 (Figures S6-S9). AFM-IR results illustrating film height profiles as well as IR chemical maps of a region in ZIF-8 and ZIF-8<sub>q</sub> films are presented in Figures S10 and S11, respectively.

We also performed experiments of tracking IR spectra as a function of temperature to eliminate the possibility of the peak at 1585 cm<sup>-1</sup> coming from extra 2mIm present in ZIF-8 cages. If the latter would be the case, this peak would reduce in intensity when heating up to temperatures above 473 K, based on TGA analysis on ZIF-8 by different authors,

including Attwa et al.<sup>65</sup>, that have reported the loss of such unreacted species at 473 K. When we heated the ZIF- $8_q$  film in UHV environment up to 523 K, we did not observe a reduction in 1585 cm<sup>-1</sup> peak intensity (See Figure S12), while some reduction in other peaks from ZIF-8 were observed. This indicates that the experimental IR peak at 1585 cm<sup>-1</sup> is not related to unreacted 2mIm trapped during the synthesis process. Additionally, the presence of unreacted 2mIm would be accompanied by a peak related to -NH stretching vibration at around 3400 cm<sup>-1</sup>, which is shown in simulations but not observed in the experimental data (Figure 5).



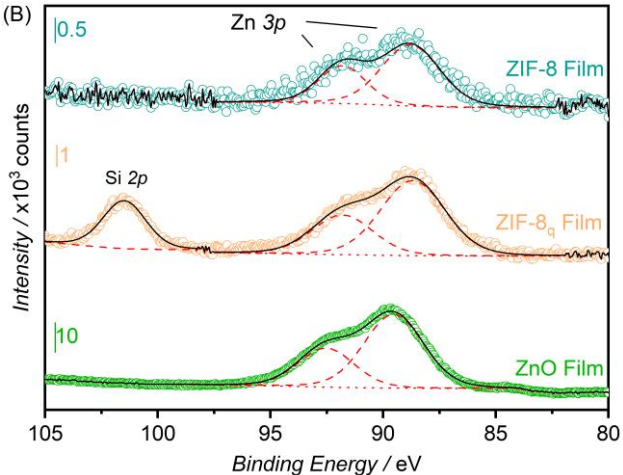


Figure 6: (A) IRRA spectra of ZIF-8 films synthesized in a Teflon-based reactor (ZIF-8 Film, No Si contamination) and a Quartz-based reactor (ZIF-8q Film, possible Si contamination) and FTIR spectrum of ZIF-8 powder. The in-set shows an enlarged view of IR spectra for the 2350-2550 cm $^{-1}$  region. (B) High-resolution XPS data showing the Si 2p and Zn 3p regions for ZIF-8 Film, ZIF-8 $_{\rm q}$  Film, and ZnO (top to bottom). Red-dashed and Red-dotted line represent fitted components and background, respectively. Black-solid line represent accumulated intensity of fitted XPS data while raw data is shown by hollow circles. Note the difference in scale bars.

Furthermore, we observe additional peaks around 1260, 1090 and 800 cm $^{-1}$  from ZIF-8 $_{\rm q}$  films, which we did not observe in any of the ZIF-8 variants we simulated. We propose that they can be assigned to Si-CH $_{\rm 3}$  and Si-O vibrational modes. Figure 6(B) presents high-resolution Si 2p and Zn 3p spectra of ZnO deposited using ALD method. While no Si

2p signal was observed from ZnO-coated wafers (labeled as ZnO Film), Figure 6(B) confirms the emergence of a strong Si signal after 2mIm vapor treatment of ZnO-wafers using the quartz-reactor, whereas such peak is not present in the ZIF-8 films made in the Teflon reactor. To assess the possibility of Si signal coming from the cracks in the Au-coating, we deposited  $\sim 15$  nm of  $ZrO_2$  on top Au-Si substrate as a barrier layer by the ALD method. Figure S13 shows highresolution Si 2p and Zn 3p spectra for a ZIF-8<sub>q</sub> film synthesized with a ZrO<sub>2</sub> barrier layer deposited between Au-Si and ZnO and further supports that the presence of Si signal after 2mIm exposure in our quartz reactor does not come from the support but rather the environment, most probably stemming from the presence of silicone vacuum grease or silicone O-rings commonly used in vacuum systems. Stassen et al. 16 and Kräuter et al. 54 have also observed the peaks at 1260, 1090 and 800 cm<sup>-1</sup> from ZIF-8 films synthesized using vapor-based method. While we could not find assignments for these peaks in the report by Stassen et al.16, Kräuter et al. 54 have assigned all three peaks (1260 cm<sup>-1</sup>, 1065 cm<sup>-1</sup> & 805 cm<sup>-1</sup>) to Si-O occurring due to the native oxide of Si substrate, which is in disagreement with the reports by Johnson et al.66 who have assigned the peak at 1260 cm-1 to -CH3 deformation from Si-CH<sub>3</sub>, 1020-1070 cm<sup>-1</sup> to Si-O-Si stretching, and around 800 cm<sup>-1</sup> to -CH<sub>3</sub> rocking and Si-C stretching in Si-CH<sub>3</sub>. We therefore propose that, in ZIF-8<sub>0</sub> film case, the peak at 1260 cm<sup>-1</sup> and the broad feature around 1090 cm<sup>-1</sup> and 800 cm<sup>-1</sup> are due to Si-CH<sub>3</sub> and S-O-Si vibrational modes originating from material generated from the siloxane copolymer, commonly utilized in vacuum grease, transported to, and deposited on the ZIF-8q film during 2mIm vapor treatment. The presence of such surface contamination could affect performance of membranes and other uses and should be eliminated.

#### 4. CONCLUSIONS

Using a combination of simulations and experimental IR measurements, we systematically assign vibrational modes for ZIF-8 structure along with its defective variants. We attempted to resolve several controversies in the earlier literature. We have also provided atoms' displacement vectors and animations corresponding to each IR peak to visualize ZIF-8 IR vibrational modes for *defect-free* as well as *defective* variants.

We suggest that the peak around 1585 cm<sup>-1</sup> indicates localized missing-metal sites. We further report that contamination from Si present in O-rings and/or vacuum grease could result in a peak around 1260 cm<sup>-1</sup>, which is not a ZIF-8 peak.

#### ASSOCIATED CONTENT

Supporting Information. Table containing information related to vibrational peak assignments, Zero-Kelvin line plots, Simulated IR spectra for the full 4000-800 cm<sup>-1</sup> range, IRRAS of amorphous ZIF-8 films and XPS of ZIF-8 films. Also included animations and simulated data in .zip folder. This material is available free of charge via the Internet at http://pubs.acs.org.

#### **AUTHOR INFORMATION**

**Corresponding Authors** 

\*J. Anibal Boscoboinik: <a href="mailto:iboscoboinik@bnl.gov">iboscoboinik@bnl.gov</a>

\*J. Ilja Siepmann: <u>siepmann@umn.edu</u>

\*M. Tsapatsis: tsapatsis@jhu.edu

#### **AUTHOR CONTRIBUTION**

M.T., J.A.B., and J.I.S. conceived and directed the project. M.A. and J.A.B. performed the IRRAS experiments, GIXD characterization, and XPS data analysis. R.P., P., and J.I.S. modeled the ZIF-8 systems and analyzed simulated IR results. M.A. and D.T.L. synthesized ZIF-8 films and performed SEM imaging. D.T.L. synthesized ZIF-8 powder and obtained IR and XRD results. S.A.T. and A.K. performed AFM-IR analysis while P.C. contributed to discussions and the determination of certain peak assignments. D.N. and X.T. assisted in obtaining GIXD and XPS data. The manuscript was written by M.A. under the guidance of J.A.B., J.I.S. and M.T. and with input

from all authors. All authors have given approval to the final version of the manuscript.

\*M.A. and R.P. contributed equally.

#### **ACKNOWLEDGMENT**

This work supported by the U.S. Department of Energy, Office of Science, Office of Basic Energy Sciences, Division of Chemical Sciences, Geosciences and Biosciences under Awards DE-SC0021212, DE-SC0021304, and DE-SC0021268 (Separation Science Program). Computational resources, in part, were provided by the Minnesota Supercomputing Institute at the University of Minnesota. Materials characterization work was carried out at the Center for Functional Nanomaterials (CFN) at Brookhaven National Laboratory, supported by the U.S. Department of Energy, Office of Basic Energy Sciences, under contract no. DE-SC0012704. We thank Fernando Camino, Gwen Wright, Kim Kisslinger, and Chang-Yong Nam for their help in using instruments at CFN.

- (1) Rowsell, J. L. C.; Yaghi, O. M. Metal–organic frameworks: a new class of porous materials. *Micropor Mesopor Mat* **2004**, 73 (1-2), 3-14. DOI: 10.1016/j.micromeso.2004.03.034.
- (2) Yaghi, O. M.; Li, G. M.; Li, H. L. Selective Binding and Removal of Guests in a Microporous Metal-Organic Framework. *Nature* **1995**, *378* (6558), 703-706. DOI: DOI 10.1038/378703a0.
- (3) Yaghi, O. M.; O'Keeffe, M.; Ockwig, N. W.; Chae, H. K.; Eddaoudi, M.; Kim, J. Reticular synthesis and the design of new materials. *Nature* **2003**, *423* (6941), 705-714. DOI: 10.1038/nature01650 (accessed 2023-12-30T11:21:01).
- (4) Horcajada, P.; Gref, R.; Baati, T.; Allan, P. K.; Maurin, G.; Couvreur, P.; Ferey, G.; Morris, R. E.; Serre, C. Metal-organic frameworks in biomedicine. *Chem Rev* **2012**, *112* (2), 1232-1268. DOI: 10.1021/cr200256v.
- (5) Cavka, J. H.; Jakobsen, S.; Olsbye, U.; Guillou, N.; Lamberti, C.; Bordiga, S.; Lillerud, K. P. A new zirconium inorganic building brick forming metal organic frameworks with exceptional stability. *J Am Chem Soc* **2008**, *130* (42), 13850-13851. DOI: 10.1021/ja8057953.
- (6) McDonald, T. M.; Mason, J. A.; Kong, X.; Bloch, E. D.; Gygi, D.; Dani, A.; Crocella, V.; Giordanino, F.; Odoh, S. O.; Drisdell, W. S.; et al. Cooperative insertion of CO2 in diamine-appended metal-organic frameworks. *Nature* **2015**, *519* (7543), 303-308. DOI: 10.1038/nature14327.
- (7) Park, K. S.; Ni, Z.; Cote, A. P.; Choi, J. Y.; Huang, R.; Uribe-Romo, F. J.; Chae, H. K.; O'Keeffe, M.; Yaghi, O. M. Exceptional chemical and thermal stability of zeolitic imidazolate frameworks. *Proc Natl Acad Sci U S A* **2006**, *103* (27), 10186-10191. DOI: 10.1073/pnas.0602439103 (acccessed 2023-05-02T14:57:08).
- (8) Pan, Y.; Liu, Y.; Zeng, G.; Zhao, L.; Lai, Z. Rapid synthesis of zeolitic imidazolate framework-8 (ZIF-8) nanocrystals in an aqueous system. *Chem Commun (Camb)* **2011**, *47* (7), 2071-2073. DOI: 10.1039/c0cc05002d (acccessed 2023-12-30T05:29:59).
- (9) Kida, K.; Okita, M.; Fujita, K.; Tanaka, S.; Miyake, Y. Formation of high crystalline ZIF-8 in an aqueous solution. *Crystengcomm* **2013**, *15* (9), 1794-1801. DOI: 10.1039/c2ce26847g (acccessed 2023-05-02T15:52:09).
- (10) Bux, H.; Liang, F.; Li, Y.; Cravillon, J.; Wiebcke, M.; Caro, J. Zeolitic imidazolate framework membrane with molecular sieving properties by microwave-assisted solvothermal synthesis. *J Am Chem Soc* **2009**, *131* (44), 16000-16001. DOI: 10.1021/ja907359t.
- (11) Shah, M. N.; Gonzalez, M. A.; McCarthy, M. C.; Jeong, H. K. An unconventional rapid synthesis of high performance metal-organic framework membranes. *Langmuir* **2013**, *29* (25), 7896-7902. DOI: 10.1021/la4014637 (accessed 2023-05-02T15:21:27).
- (12) Pan, Y. C.; Li, T.; Lestari, G.; Lai, Z. P. Effective separation of propylene/propane binary mixtures by ZIF-8 membranes. *Journal of Membrane Science* **2012**, *390*, 93-98. DOI: 10.1016/j.memsci.2011.11.024.
- (13) Brown, A. J.; Brunelli, N. A.; Eum, K.; Rashidi, F.; Johnson, J. R.; Koros, W. J.; Jones, C. W.; Nair, S. Separation membranes. Interfacial microfluidic processing of metalorganic framework hollow fiber membranes. *Science* **2014**, *345* (6192), 72-75. DOI: 10.1126/science.1251181.
- (14) Ma, X.; Kumar, P.; Mittal, N.; Khlyustova, A.; Daoutidis, P.; Mkhoyan, K. A.; Tsapatsis, M. Zeolitic imidazolate framework membranes made by ligand-induced

- permselectivation. *Science* **2018**, *361* (6406), 1008-1011. DOI: 10.1126/science.aat4123 (acccessed 2023/05/02).
- (15) Dai, H.; Yuan, X. Z.; Jiang, L. B.; Wang, H.; Zhang, J.; Zhang, J. J.; Xiong, T. Recent advances on ZIF-8 composites for adsorption and photocatalytic wastewater pollutant removal: Fabrication, applications and perspective. *Coordin Chem Rev* **2021**, *441*. DOI: ARTN 213985 10.1016/j.ccr.2021.213985.
- (16) Stassen, I.; Styles, M.; Grenci, G.; Gorp, H. V.; Vanderlinden, W.; Feyter, S. D.; Falcaro, P.; Vos, D. D.; Vereecken, P.; Ameloot, R. Chemical vapour deposition of zeolitic imidazolate framework thin films. *Nat Mater* **2016**, *15* (3), 304-310. DOI: 10.1038/nmat4509 (acccessed 2023-05-03T11:05:24).
- (17) Lee, Y. R.; Kim, J.; Ahn, W. S. Synthesis of metal-organic frameworks: A mini review. *Korean Journal of Chemical Engineering* **2013**, *30* (9), 1667-1680. DOI: 10.1007/s11814-013-0140-6 (acccessed 2023-12-07T10:07:30).
- (18) Lee, Y.-R.; Jang, M.-S.; Cho, H.-Y.; Kwon, H.-J.; Kim, S.; Ahn, W.-S. ZIF-8: A comparison of synthesis methods. *Chemical Engineering Journal* **2015**, *271*, 276-280. DOI: 10.1016/j.cej.2015.02.094.
- (19) Jin, B.; Wang, S.; Boglaienko, D.; Zhang, Z.; Zhao, Q.; Ma, X.; Zhang, X.; De Yoreo, J. J. The role of amorphous ZIF in ZIF-8 crystallization kinetics and morphology. *Journal of Crystal Growth* **2023**, *603*. DOI: 10.1016/j.jcrysgro.2022.126989.
- (20) Phan, A.; Doonan, C. J.; Uribe-Romo, F. J.; Knobler, C. B.; O'Keeffe, M.; Yaghi, O. M. Synthesis, structure, and carbon dioxide capture properties of zeolitic imidazolate frameworks. *Acc Chem Res* **2010**, *43* (1), 58-67. DOI: 10.1021/ar900116g.
- (21) D'Alessandro, D. M.; Smit, B.; Long, J. R. Carbon dioxide capture: prospects for new materials. *Angew Chem Int Ed Engl* **2010**, *49* (35), 6058-6082. DOI: 10.1002/anie.201000431 (acccessed 2024-01-03T01:22:53).
- (22) Lee, D. T.; Corkery, P.; Park, S.; Jeong, H. K.; Tsapatsis, M. Zeolitic Imidazolate Framework Membranes: Novel Synthesis Methods and Progress Toward Industrial Use. *Annu Rev Chem Biomol Eng* **2022**, *13* (1), 529-555. DOI: 10.1146/annurev-chembioeng-092320-120148 (acccessed 2023-08-08T23:54:37).
- (23) Liu, D. F.; Ma, X. L.; Xi, H. X.; Lin, Y. S. Gas transport properties and propylene/propane separation characteristics of ZIF-8 membranes. *Journal of Membrane Science* **2014**, *451*, 85-93. DOI: 10.1016/j.memsci.2013.09.029.
- (24) Li, H.; Li, L.; Lin, R.-B.; Zhou, W.; Zhang, Z.; Xiang, S.; Chen, B. Porous metal-organic frameworks for gas storage and separation: Status and challenges. *EnergyChem* **2019**, *1* (1), 100006. DOI: 10.1016/j.enchem.2019.100006.
- (25) Heinz, K.; Rogge, S. M. J.; Kalytta-Mewes, A.; Volkmer, D.; Bunzen, H. MOFs for long-term gas storage: exploiting kinetic trapping in ZIF-8 for on-demand and stimulicontrolled gas release. *Inorganic Chemistry Frontiers* **2023**, *10* (16), 4763-4772. DOI: 10.1039/d3qi01007d (acccessed 2023-12-07T10:30:25).
- (26) Farrusseng, D.; Aguado, S.; Pinel, C. Metal-organic frameworks: opportunities for catalysis. *Angew Chem Int Ed Engl* **2009**, *48* (41), 7502-7513. DOI: 10.1002/anie.200806063 (acccessed 2023-12-07T09:44:24).
- (27) Wang, Q.; Sun, Y.; Li, S.; Zhang, P.; Yao, Q. Synthesis and

- modification of ZIF-8 and its application in drug delivery and tumor therapy. *RSC Adv* **2020**, *10* (62), 37600-37620. DOI: 10.1039/d0ra07950b (acccessed 2023-05-02T15:15:47).
- (28) Lu, G.; Hupp, J. T. Metal-organic frameworks as sensors: a ZIF-8 based Fabry-Perot device as a selective sensor for chemical vapors and gases. *J Am Chem Soc* **2010**, *132* (23), 7832-7833. DOI: 10.1021/ja101415b (acccessed 2023-12-07T09:33:52).
- (29) Zhang, C.; Han, C.; Sholl, D. S.; Schmidt, J. R. Computational Characterization of Defects in Metal-Organic Frameworks: Spontaneous and Water-Induced Point Defects in ZIF-8. *J Phys Chem Lett* **2016**, *7* (3), 459-464. DOI: 10.1021/acs.jpclett.5b02683 (acccessed 2023-05-18T20:02:44).
- (30) Cheng, P. F.; Hu, Y. H.  $H_2O$ -Functionalized Zeolitic  $Zn(2-methylimidazole)_2$  Framework (ZIF-8) for  $H_2$  Storage. *J Phys Chem C* **2014**, *118* (38), 21866-21872. DOI: 10.1021/jp507030g (acccessed 2023-06-01T21:30:57).
- (31) Lee, M. J.; Kwon, H. T.; Jeong, H. K. Defect-dependent stability of highly propylene-selective zeolitic-imidazolate framework ZIF-8 membranes. *Journal of Membrane Science* **2017**, *529*, 105-113. DOI: 10.1016/j.memsci.2016.12.068 (accessed 2023-05-18T20:04:53).
- (32) Perrot, V.; Roussey, A.; Benayad, A.; Veillerot, M.; Mariolle, D.; Sole-Daura, A.; Mellot-Draznieks, C.; Ricoul, F.; Canivet, J.; Quadrelli, E. A.; Jousseaume, V. ZIF-8 thin films by a vapor-phase process: limits to growth. *Nanoscale* **2023**, *15* (15), 7115-7125. DOI: 10.1039/d3nr00404j (acccessed 2023-06-27T15:48:53).
- (33) Tian, F. Y.; Cerro, A. M.; Mosier, A. M.; Wayment-Steele, H. K.; Shine, R. S.; Park, A.; Webster, E. R.; Johnson, L. E.; Johal, M. S.; Benz, L. Surface and Stability Characterization of a Nanoporous ZIF-8 Thin Film. *J Phys Chem C* **2014**, *118* (26), 14449-14456. DOI: 10.1021/jp5041053.
- (34) Jung, G.; Jung, S. G.; Cole, J. M. Automatic materials characterization from infrared spectra using convolutional neural networks. *Chem Sci* **2023**, *14* (13), 3600-3609. DOI: 10.1039/d2sc05892h (acccessed 2023-09-18T07:11:34).
- (35) Hadjiivanov, K. I.; Panayotov, D. A.; Mihaylov, M. Y.; Ivanova, E. Z.; Chakarova, K. K.; Andonova, S. M.; Drenchev, N. L. Power of Infrared and Raman Spectroscopies to Characterize Metal-Organic Frameworks and Investigate Their Interaction with Guest Molecules. *Chem Rev* **2021**, *121* (3), 1286-1424. DOI: 10.1021/acs.chemrev.0c00487 (acccessed 2023-05-03T10:54:37).
- (36) Miao, Y.; Lee, D. T.; de Mello, M. D.; Ahmad, M.; Abdel-Rahman, M. K.; Eckhert, P. M.; Boscoboinik, J. A.; Fairbrother, D. H.; Tsapatsis, M. Solvent-free bottom-up patterning of zeolitic imidazolate frameworks. *Nat Commun* **2022**, *13* (1), 420. DOI: 10.1038/s41467-022-28050-z (acccessed 2023-06-02T08:12:46).
- (37) Dorneles de Mello, M.; Ahmad, M.; Lee, D. T.; Dimitrakellis, P.; Miao, Y.; Zheng, W.; Nykypanchuk, D.; Vlachos, D. G.; Tsapatsis, M.; Boscoboinik, J. A. In Situ Tracking of Nonthermal Plasma Etching of ZIF-8 Films. *ACS Appl Mater Interfaces* **2022**, *14* (16), 19023-19030. DOI: 10.1021/acsami.2c00259 (acccessed 2023-06-02T08:13:08).
- (38) Miao, Y.; Lee, D. T.; Dorneles de Mello, M.; Abdel-Rahman, M. K.; Corkery, P.; Boscoboinik, J. A.; Fairbrother, D. H.; Tsapatsis, M. Electron beam induced modification of ZIF-8 membrane permeation properties. *Chem Commun* (*Camb*) **2021**, *57* (43), 5250-5253. DOI:

- 10.1039/d1cc00252j.
- (39) Kuhne, T. D.; Iannuzzi, M.; Del Ben, M.; Rybkin, V. V.; Seewald, P.; Stein, F.; Laino, T.; Khaliullin, R. Z.; Schutt, O.; Schiffmann, F.; et al. CP2K: An electronic structure and molecular dynamics software package Quickstep: Efficient and accurate electronic structure calculations. *J Chem Phys* **2020**, *152* (19), 194103. DOI: 10.1063/5.0007045 (acccessed 5/2/2023).
- (40) Perdew, J. P.; Burke, K.; Ernzerhof, M. Generalized Gradient Approximation Made Simple. *Phys Rev Lett* **1996**, 77 (18), 3865-3868. DOI: 10.1103/PhysRevLett.77.3865.
- (41) Grimme, S.; Antony, J.; Ehrlich, S.; Krieg, H. A consistent and accurate ab initio parametrization of density functional dispersion correction (DFT-D) for the 94 elements H-Pu. *J Chem Phys* **2010**, *132* (15), 154104. DOI: 10.1063/1.3382344 (accessed 5/2/2023).
- (42) VandeVondele, J.; Krack, M.; Mohamed, F.; Parrinello, M.; Chassaing, T.; Hutter, J. QUICKSTEP: Fast and accurate density functional calculations using a mixed Gaussian and plane waves approach. *Computer Physics Communications* **2005**, *167* (2), 103-128. DOI: 10.1016/j.cpc.2004.12.014 (accessed 2023-05-02T15:39:18).
- (43) Goedecker, S.; Teter, M.; Hutter, J. Separable dual-space Gaussian pseudopotentials. *Phys Rev B Condens Matter* **1996**, *54* (3), 1703-1710. DOI: 10.1103/physrevb.54.1703 (accessed 2023-05-02T15:39:59).
- (44) Thomas, M.; Brehm, M.; Fligg, R.; Vohringer, P.; Kirchner, B. Computing vibrational spectra from ab initio molecular dynamics. *Phys Chem Chem Phys* **2013**, *15* (18), 6608-6622. DOI: 10.1039/c3cp44302g (acccessed 2023-05-02T15:41:05).
- (45) Brehm, M.; Kirchner, B. TRAVIS a free analyzer and visualizer for Monte Carlo and molecular dynamics trajectories. *J Chem Inf Model* **2011**, *51* (8), 2007-2023. DOI: 10.1021/ci200217w (accessed 2023-05-02T16:07:26).
- (46) Kresse, G.; Furthmuller, J. Efficient iterative schemes for ab initio total-energy calculations using a plane-wave basis set. *Phys Rev B Condens Matter* **1996**, *54* (16), 11169-11186. DOI: 10.1103/physrevb.54.11169 (acccessed 2023-06-01T21:05:56).
- (47) Kresse, G.; Hafner, J. Ab initio molecular dynamics for liquid metals. *Phys Rev B Condens Matter* **1993**, 47 (1), 558-561. DOI: 10.1103/physrevb.47.558 (acccessed 2023-06-01T21:07:14).
- (48) Zhang, Y.; Jia, Y.; Hou, L. Synthesis of zeolitic imidazolate framework-8 on polyester fiber for PM(2.5) removal. *RSC Adv* **2018**, *8* (55), 31471-31477. DOI: 10.1039/c8ra06414h (accessed 2023-05-03T11:02:32).
- (49) Liu, J.; He, J.; Wang, L.; Li, R.; Chen, P.; Rao, X.; Deng, L.; Rong, L.; Lei, J. NiO-PTA supported on ZIF-8 as a highly effective catalyst for hydrocracking of Jatropha oil. *Sci Rep* **2016**, *6* (1), 23667. DOI: 10.1038/srep23667 (acccessed 2023-06-02T08:12:18).
- (50) Nozari, V.; Calahoo, C.; Tuffnell, J. M.; Keen, D. A.; Bennett, T. D.; Wondraczek, L. Ionic liquid facilitated melting of the metal-organic framework ZIF-8. *Nat Commun* **2021**, *12* (1), 5703. DOI: 10.1038/s41467-021-25970-0 (acccessed 2023-06-02T08:11:43).
- (51) dos Santos Ferreira da Silva, J.; Lopez Malo, D.; Anceski Bataglion, G.; Nogueira Eberlin, M.; Machado Ronconi, C.; Alves Junior, S.; de Sa, G. F. Adsorption in a Fixed-Bed Column and Stability of the Antibiotic Oxytetracycline Supported on Zn(II)-[2-Methylimidazolate] Frameworks in Aqueous Media. *PLoS One* **2015**, *10* (6), e0128436. DOI:

- 10.1371/journal.pone.0128436 (acccessed 2023-06-02T08:12:34).
- (52) Zhao, Y.; Wei, Y.; Lyu, L.; Hou, Q.; Caro, J.; Wang, H. Flexible Polypropylene-Supported ZIF-8 Membranes for Highly Efficient Propene/Propane Separation. *J Am Chem Soc* **2020**, *142* (50), 20915-20919. DOI: 10.1021/jacs.0c07481 (acccessed 2023-06-02T08:10:51). (53) Md Nordin, N. A. H.; Racha, S. M.; Matsuura, T.; Misdan, N.; Abdullah Sani, N. A.; Ismail, A. F.; Mustafa, A. Facile modification of ZIF-8 mixed matrix membrane for CO2/CH4 separation: synthesis and preparation. *RSC Advances* **2015**, 5 (54), 43110-43120. DOI: 10.1039/c5ra02230d (acccessed 2023-06-02T08:11:27).
- (54) Kräuter, M.; Cruz, A. J.; Stassin, T.; Rodríguez-Hermida, S.; Ameloot, R.; Resel, R.; Coclite, A. M. Influence of Precursor Density and Conversion Time on the Orientation of Vapor-Deposited ZIF-8. *Crystals* **2022**, *12* (2), 217. DOI: 10.3390/cryst12020217.
- (55) Xu, B.; Mei, Y.; Xiao, Z.; Kang, Z.; Wang, R.; Sun, D. Monitoring thermally induced structural deformation and framework decomposition of ZIF-8 through in situ temperature dependent measurements. *Physical Chemistry Chemical Physics* **2017**, *19* (40), 27178-27183. DOI: 10.1039/c7cp04694d (accessed 2023-11-07T17:06:36).
- (56) Moslein, A. F.; Dona, L.; Civalleri, B.; Tan, J. C. Defect Engineering in Metal-Organic Framework Nanocrystals: Implications for Mechanical Properties and Performance. *ACS Appl Nano Mater* **2022**, *5* (5), 6398-6409. DOI: 10.1021/acsanm.2c00493 (acccessed 2023-05-03T11:24:33).
- (57) Xiong, T.; Zhang, Y.; Donà, L.; Gutiérrez, M.; Möslein, A. F.; Babal, A. S.; Amin, N.; Civalleri, B.; Tan, J. C. Tunable Fluorescein-Encapsulated Zeolitic Imidazolate Framework-8 Nanoparticles for Solid-State Lighting. *Acs Applied Nano Materials* **2021**, *4* (10), 10321-10333. DOI: 10.1021/acsanm.1c01829 (acccessed 2023-11-13T06:31:10).
- (58) Bergaoui, M.; Khalfaoui, M.; Awadallah-F, A.; Al-Muhtaseb, S. A review of the features and applications of ZIF-8 and its derivatives for separating CO2 and isomers of C3- and C4- hydrocarbons. *Journal of Natural Gas Science and Engineering* **2021**, *96*, 104289. DOI: 10.1016/j.jngse.2021.104289.
- (59) Jafari, S.; Ghorbani-Shahna, F.; Bahrami, A.; Kazemian, H. Effects of Post-Synthesis Activation and Relative

- Humidity on Adsorption Performance of ZIF-8 for Capturing Toluene from a Gas Phase in a Continuous Mode. *Applied Sciences-Basel* **2018**, *8* (2), 310. DOI: ARTN 310 10.3390/app8020310 (accessed 2023-12-08T14:32:34). (60) Deacon, A.; Briquet, L.; Malankowska, M.; Massingberd-Mundy, F.; Rudic, S.; Hyde, T. L.; Cavaye, H.; Coronas, J.; Poulston, S.; Johnson, T. Understanding the ZIF-L to ZIF-8 transformation from fundamentals to fully costed kilogram-scale production. *Commun Chem* **2022**, *5* (1), 18. DOI: 10.1038/s42004-021-00613-z (accessed 2023-12-30T01:32:58).
- (61) Edzards, J.; Sassnick, H. D.; Buzanich, A. G.; Valencia, A. M.; Emmerling, F.; Beyer, S.; Cocchi, C. Effects of Ligand Substituents on the Character of Zn-Coordination in Zeolitic Imidazolate Frameworks. *J Phys Chem C* **2023**, *127* (43), 21456-21464. DOI: 10.1021/acs.jpcc.3c06054.
- (62) Gerardi, H. K.; Gardenier, G. H.; Viswanathan, U.; Auerbach, S. M.; Johnson, M. A. Vibrational predissociation spectroscopy and theory of Ar-tagged, protonated Imidazole (Im)  $Im_{1-3}H^+\cdot Ar$  clusters. *Chem Phys Lett* **2011**, 501 (4-6), 172-178. DOI: 10.1016/j.cplett.2010.10.062.
- (63) Kwon, H. T.; Jeong, H. K.; Lee, A. S.; An, H. S.; Lee, J. S. Heteroepitaxially grown zeolitic imidazolate framework membranes with unprecedented propylene/propane separation performances. *J Am Chem Soc* **2015**, *137* (38), 12304-12311. DOI: 10.1021/jacs.5b06730 From NLM Medline.
- (64) Tanaka, S.; Tanaka, Y. A Simple Step toward Enhancing Hydrothermal Stability of ZIF-8. *ACS Omega* **2019**, *4* (22), 19905-19912. DOI: 10.1021/acsomega.9b02812 (acccessed 2024-04-14T22:28:47).
- (65) Attwa, M.; Said, A.; Elgamal, M.; El-Shaer, Y.; Elbasuney, S. Bespoke Energetic Zeolite Imidazolate Frameworks-8 (ZIF-8)/Ammonium Perchlorate Nanocomposite: A Novel Reactive Catalyzed High Energy Dense Material with Superior Decomposition Kinetics. *Journal of Inorganic and Organometallic Polymers and Materials* **2024**, *34* (1), 387-400. DOI: 10.1007/s10904-023-02834-2 (acccessed 2024-04-10T14:23:54).
- (66) Johnson, L. M.; Gao, L.; Shields, I. C.; Smith, M.; Efimenko, K.; Cushing, K.; Genzer, J.; Lopez, G. P. Elastomeric microparticles for acoustic mediated bioseparations. *J Nanobiotechnology* **2013**, *11* (1), 22. DOI: 10.1186/1477-3155-11-22 (accessed 2023-08-10T00:52:33).

